ARMY RESEARCH LABORATORY

Lightweight, Durable Army Antennas Using Carbon Nanotube Technology (First-year Report)

by Steven D. Keller, Amir I. Zaghloul, and Barbara Nichols

ARL-MR-0803 **January 2012**

NOTICES

Disclaimers

The findings in this report are not to be construed as an official Department of the Army position unless so designated by other authorized documents.

Citation of manufacturer's or trade names does not constitute an official endorsement or approval of the use thereof.

Destroy this report when it is no longer needed. Do not return it to the originator.

Army Research Laboratory
Adelphi, MD 20783-1197

ARL-MR-0803 **January 2012**

Lightweight, Durable Army Antennas Using Carbon Nanotube Technology (First-year Report)

Steven D. Keller, Amir I. Zaghloul, and Barbara Nichols
Sensors and Electron Devices Directorate, ARL

REPORT DOCUMENTATION PAGE			Form Approved OMB No. 0704-0188

1. REPORT DATE *(DD-MM-YYYY)*	2. REPORT TYPE	3. DATES COVERED (From - To)
January 2012	DRI	1 October 2010 to 30 September 2011

4. TITLE AND SUBTITLE	5a. CONTRACT NUMBER
Lightweight, Durable Army Antennas Using Carbon Nanotube Technology (First-year Report)	5b. GRANT NUMBER
	5c. PROGRAM ELEMENT NUMBER
6. AUTHOR(S)	5d. PROJECT NUMBER
Steven D. Keller, Amir I. Zaghloul, and Barbara Nichols	FY11-SED-028
	5e. TASK NUMBER
	5f. WORK UNIT NUMBER
7. PERFORMING ORGANIZATION NAME(S) AND ADDRESS(ES)	8. PERFORMING ORGANIZATION REPORT NUMBER
U.S. Army Research Laboratory ATTN: RDRL-SER-M Adelphi, MD 20783-1197	ARL-MR-0803
9. SPONSORING/MONITORING AGENCY NAME(S) AND ADDRESS(ES)	10. SPONSOR/MONITOR'S ACRONYM(S)
	11. SPONSOR/MONITOR'S REPORT NUMBER(S)

12. DISTRIBUTION/AVAILABILITY STATEMENT

Approved for public release; distribution unlimited.

13. SUPPLEMENTARY NOTES

14. ABSTRACT

The application of carbon nanotube (CNT) materials to produce lightweight, flexible, and durable alternatives to existing and future Army antenna designs is explored through simulation and material fabrication and characterization. The conductivity and current distribution for a dipole antenna constructed from CNT thread/rope are simulated using Hallén's integral equation for a thin wire applied to the method of moments. A variety of CNT thread/rope samples are fabricated and their physical and electrical characteristics are measured and compared with the simulation results. Finally, to support future nanoscale antenna array research, the first steps towards establishing patterned multiwall CNT (MWNT) array fabrication capabilities at the U.S. Army Research Laboratory (ARL) are attempted and documented.

15. SUBJECT TERMS

Carbon nanotube, antenna, array, dipole, Method of Moments

16. SECURITY CLASSIFICATION OF:			17. LIMITATION OF ABSTRACT	18. NUMBER OF PAGES	19a. NAME OF RESPONSIBLE PERSON
a. REPORT	b. ABSTRACT	c. THIS PAGE			Steven D. Keller
Unclassified	Unclassified	Unclassified	UU	42	19b. TELEPHONE NUMBER (*Include area code*) (301) 394-0576

Standard Form 298 (Rev. 8/98)
Prescribed by ANSI Std. Z39.18

Contents

List of Figures

List of Tables

Acknowledgments

We thank Dr. Vesselin Shanov, Dr. Mark Schulz, and Dr. David Mast of the NanoWorld Laboratory at the University of Cincinnati for fabricating and measuring carbon nanotube thread and rope samples for this research under U.S. Army Research Laboratory (ARL) contract number W911QX11P0132.

1. Objective

The concealment and size/weight reduction of Army sensor and communication system antennas is currently an important thrust in Army research. Many new wireless systems that are added to an Army vehicle or a Soldier's communications gear yield significant additional weight to the platform. Additionally, many proposed conformal body-worn antennas constructed from standard bulk materials such as copper fail to stand up to significant "wear-and-tear" due to lack of durability and thus are limited in their placement to areas on the body that see minimal flexing and bending. There is a critical need for lightweight, low-profile and durable antennas that can be seamlessly integrated into vehicular Army platforms and/or fabricated onto the uniform of the individual Soldier. The objective of this research is to explore the latest advances in carbon nanotube (CNT) technology and how it may be applied to Army antenna systems to produce lightweight, flexible, and durable alternatives to existing and future antenna designs.

2. Approach

CNT structures have leapt to the forefront of materials research interest over the past decade due to their demonstration of a variety of attractive physical characteristics such as high durability (tensile strength exceeding 1–2 GPa) and extremely light weight in comparison with standard metallic materials such as copper and steel. In addition to possessing such valuable physical characteristics, it has been shown that CNTs may exhibit similar, and in some cases, enhanced electrical characteristics when compared with standard conductive materials such as copper (*1*). The conductivity and power efficiency of a CNT structure may be exceptionally high since its quantum resistance does not inversely scale with the square of its radius like traditional metal structures and since electrons only flow along its carbon atom shell in two parallel propagation channels, referred to as π-bands, resulting in a negligible skin effect. The application of an individual single-wall CNT (SWNT) as an antenna has been analytically shown to yield very low radiation efficiency at microwave frequencies (*2, 3*), mainly due to the large reactance resulting from quantum effects of its nanometer radius. These include quantum capacitance, C_Q = 100 aF/μm, due to the finite density of states at the Fermi energy and kinetic inductance, L_K = |16 nH/μm, due to charge-carrier inertia of the electrons flowing along the nanotube (*2*). While overall radiation efficiency of a single CNT structure may be lower than that of a traditional metal structure (since the resistance of CNT structures have been predicted to be quite high at the nanometer scale), the counter-balancing attractive physical and electrical characteristics make its use in radio frequency (RF) and antenna applications worthy of further investigation.

The electrical properties of CNTs have been applied to antenna designs by using the individual CNTs as conductors in an array format and also by harvesting individual CNTs and mixing them into a liquid to form a conductive solution. Specific examples of these applications include the fabrication of a flexible patch antenna structure from compressed CNT arrays incorporated into a polymer substrate (*4*) and a patch antenna printed onto a flexible substrate using CNT-enhanced conductive ink (*5*).

It has recently been shown through analysis (*6, 7*) and measurement (*8*) that the dominant kinetic inductance and resistance of a CNT can be significantly reduced by bringing together a large number of CNTs into a bundle structure. It has also been predicted through simulations that dipole antennas constructed from CNT bundle structures may exhibit radiation efficiency orders of magnitude higher than that of individual CNTs (*9*) and that this radiation efficiency increases as the nanotube density with the bundle is increased (*10*). Emerging fabrication techniques have made realizable the synthesis of large-scale CNT bundle structures such as threads, ribbons, and sheets. By using these CNT threads to produce wireframe antennas (dipole, loop etc.) and CNT sheets/ribbons to produce planar and waveguide antennas (patch, horn etc.), it may be possible to fabricate antennas with significantly reduced weight and enhanced flexibility/durability and power handling capabilities when compared with antenna structures fabricated out of traditional bulk conductive materials.

In order to investigate the application of CNT materials to Army antenna systems, a two-pronged approach is employed. The first approach focuses on antennas constructed from the aforementioned bulk CNT materials such as threads and sheets. Since these materials are currently available from select laboratories, it is possible to explore a variety of CNT thread dipole antennas through both simulation and measurement in this Director's Research Initiative (DRI). In Year 1, the simulated conductivity, current distribution and radiation efficiency of CNT thread dipole antennas were investigated and compared with those of an antenna constructed from traditional bulk conductive material (e.g., copper). Additionally, the conductivity, tensile strength, and weight of fully fabricated CNT thread and rope samples were measured and analyzed (section 3.1). This provides a thorough understanding of the benefits and tradeoffs associated with constructing antennas using bulk CNT materials and lays the groundwork for the fabrication and measurement of complex antenna structures from such materials, including textile-embedded dipole antennas and meshed CNT thread patch antennas, in year 2 of this DRI.

The second approach explores the possibility of using periodic arrays of CNTs embedded into a flexible substrate as the main radiating elements of a fabric-like structure, which, when incorporated as a part of the outer fabric of a garment, can function as a body-worn antenna array. The concept of this *Nanofabric* antenna system is depicted in figure 1.

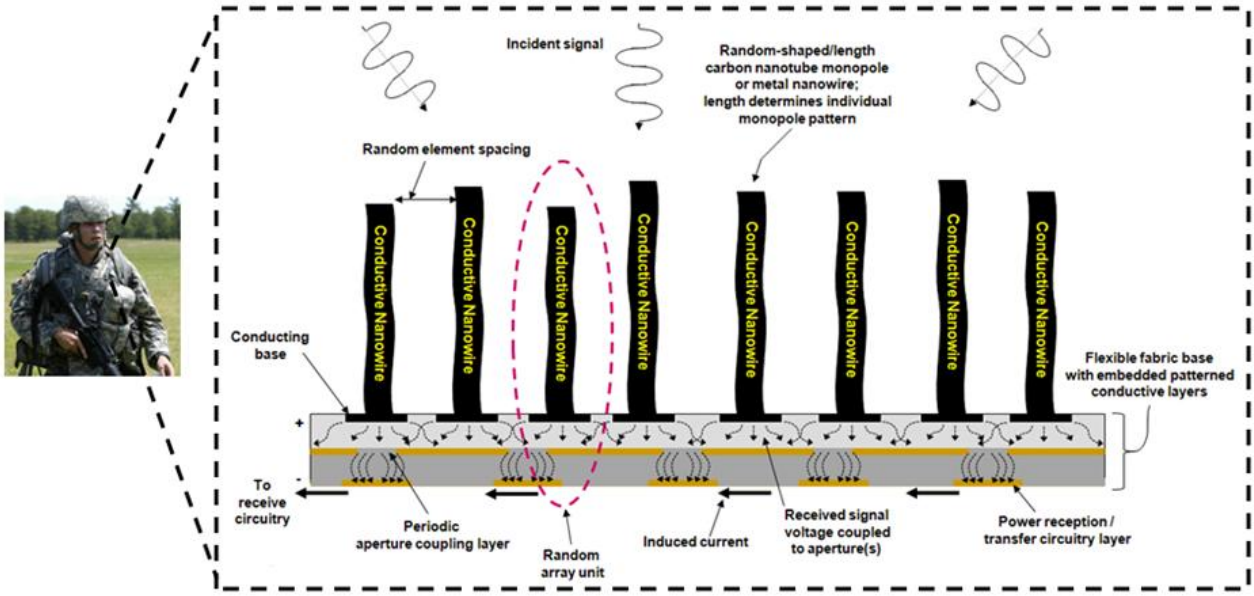

Figure 1. Conceptual diagram of the *Nanofabric* carbon nanotube antenna array.

A large number of periodically spaced conductive CNTs and/or CNT bundles are grown and embedded into a flexible substrate to form the outer surface of a fabric-like structure. The vertically-aligned CNTs form either a fixed or randomly spaced array of monopole antennas (*11*) with each element connected to a metallic seed base (as a byproduct of the growth process). The base of each CNT couples through a layer of periodic apertures to a conducting patch/power combiner network that routes the received signal to the antenna output and the integrated receiver. All layers below the monopole array are made of flexible materials, such as fabric and/or flexible polymers. Due to the durable, flexible nature of the array and the fabric-like texture exhibited by the outer skin CNT layer, the complete *Nanofabric* structure may be embedded into an Army patterned material as an integrated antenna system capable of both transmit and receive functionality.

In order to develop a functional prototype of the *Nanofabric* CNT antenna array, an accurate design approach must be developed both analytically and through electromagnetic simulation. The simulation effort that is employed to explore the CNT bundle/thread antennas for approach #1 is also directly applicable to the simulation of the *Nanofabric* antenna array. The main difference is that the simulation must be extended from a single CNT bundle to a finite array of randomly spaced single element CNTs and CNT bundles. Additionally, the in-house CNT fabrication capabilities at the U.S. Army Research Laboratory (ARL) must be advanced in a few key areas. Currently, the RDRL-SER-L branch can produce random arrays of SWNTs. A SWNT is basically a hollow tube constructed from a rolled up sheet of graphene, consisting of a lattice of carbon atoms bonded together in a hexagonal honeycomb-like structure. The axis orientation by which the graphene sheet is rolled up, known as the chirality, can lead to either semiconducting (some dual and zigzag chirality nanotubes) or metallic SWNTs (all armchair

chirality nanotubes) (*12*). Multiwall CNTs (MWNTs) consist of multiple shells of rolled up graphene sheets forming a layered hollow tube, with each shell typically separated from its neighboring shell(s) by the van der Waals gap (0.34 nm), as shown in figure 2.

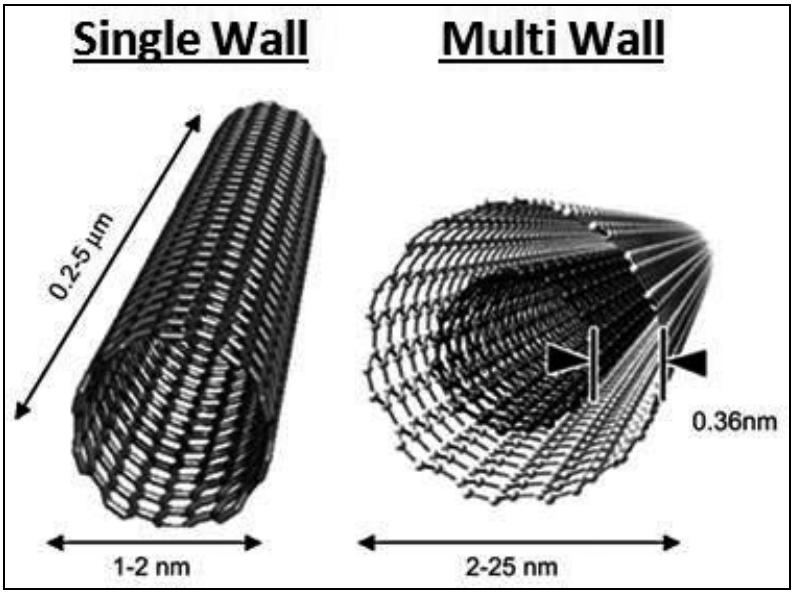

Figure 2. Typical dimensions of a SWNT and MWNT (adapted from Iijima [*13*]).

It has been experimentally shown that MWNTs mainly exhibit metallic conductivity at room temperature due to the large tube diameter resulting from the multiple shells, typically of armchair chirality (*14*). These results indicate that the use of MWNTs as the radiating elements in the *Nanofabric* antenna array will ensure that a maximum percentage of these elements exhibit high conductivity. Thus, an important step towards realizing a fully functional *Nanofabric* system is to establish patterned MWNT growth capabilities at ARL. Additionally, a method to transfer the CNT arrays onto a flexible substrate must be developed. Vertically aligned MWNT arrays can only be produced via chemical vapor deposition (CVD) using either patterned catalysts or anodized alumina templates. CVD growth will need to be optimized to produce the target nanotube length (1–2 mm at this time) as well as spacing between elements. A transfer method must be developed to encapsulate the CNTs in the grown arrays and remove them from the growth substrates. The encapsulation must then be transferred to the flexible substrates. Bonding techniques also need to be developed to ensure the CNTs will remain attached to the flexible substrates without any degradation to the tube or the array structure formation. For year 1 of this DRI, initial research into the establishment of MWNT growth capabilities at ARL is conducted (section 3.2).

3. Results

3.1 Carbon Nanotube Thread Dipole Antenna

As a first step in this investigation of antenna structures fabricated from CNT materials, a variety of half wavelength (λ/2) CNT thread dipole antennas were simulated. A conceptual diagram of a CNT thread dipole antenna is shown in figure 3. The dipole thread is composed of many thousands of individual double-wall CNTs with typical diameter of 10–12 nm held together by van der Waals forces and spun to form a strong, thread-like structure with a typical diameter of ~20–25 μm. These are connected to the output of a balun to match the unbalanced dipole load to a balanced coaxial feed connector and provide a 180° phase difference between the signal excitation in each leg of the dipole.

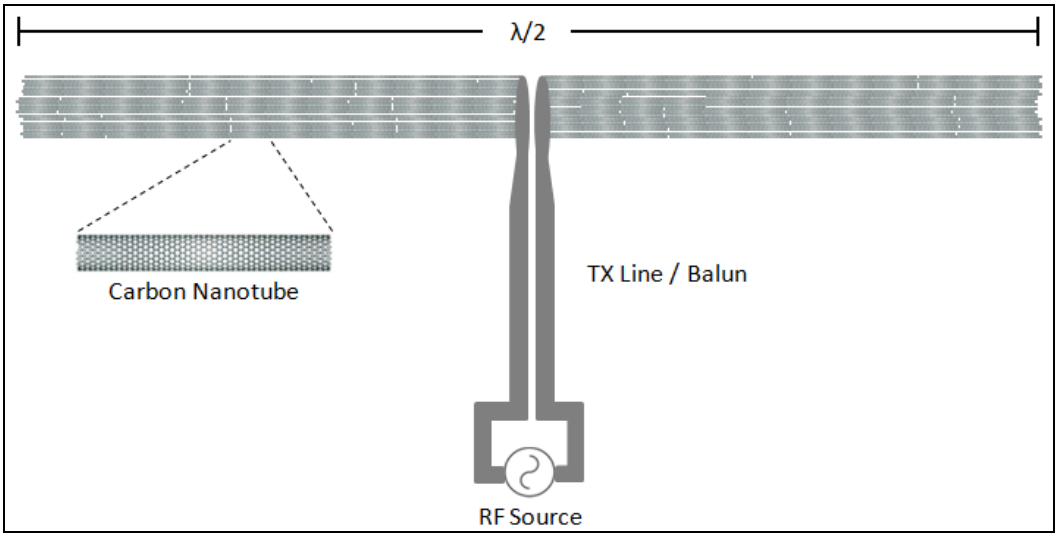

Figure 3. CNT thread dipole antenna concept.

A contract was established with the Nanoworld Laboratory at the University of Cincinnati (UC) to acquire CNT thread for the construction of these dipole antenna prototypes. Details of this fabrication process and measurements of the CNT thread prototypes are provided in section 3.1.2.

A fully fabricated single CNT thread, referred to as 1-ply thread, may be spun together with other 1-ply CNT threads to yield a larger CNT rope. This increases the overall conductor radius and number of CNTs (conductive paths) within the thread and should consequently increase the electrical performance. Prior to the contract with UC, it was possible to manufacture 1-ply CNT thread and 2- or 3-ply CNT rope. By combining three 3-ply CNT ropes, it should also be possible to fabricate a 3x3-ply (or 9-ply) CNT rope. An emphasis of the contract was to push this fabrication boundary further and explore the physical and electrical properties of larger ply

CNT rope. The simulations in section 3.1.1 investigate a 1-ply CNT thread, a 3-ply rope, a 3x3-ply CNT rope, and a CNT rope with the same diameter as 15-gauge wire (1250 μm). At this point in time, the fabrication of a CNT rope with a diameter equivalent to 15-gauge wire has not been demonstrated.

3.1.1 Simulation

In order to predict the radiation performance of a dipole antenna constructed from CNT thread, a method of moments (MoM) simulation technique was applied to Hallén's integral equation for a thin wire (*16*). The solution to the Helmholtz equation using the electric field, *E*, and magnetic wave potential, *A*, serves as the starting point of this derivation. With this, the electric field may be represented in terms of the current density, *J*,

$$E = -j\omega\mu A + \frac{1}{j\omega\varepsilon}\nabla(\nabla \cdot A), \tag{1}$$

where

$$A = \iiint \frac{Je^{-jk|r-r'|}}{4\pi\,|\,r-r'\,|}dr'. \tag{2}$$

In the above equation, *k* is the wavevector, ω is the angular frequency, ε is the permittivity, μ is the permeability, and $|r - r'|$ is the vector between a point source and a distant point in space. The current is assumed to travel axially along a wire with conductivity, σ. The surface current density, J_z, may be solved for with the general version of Ohm's law,

$$J_z = \sigma E_z. \tag{3}$$

Each of the cases that are examined here satisfy the criteria for a thin wire of half-length, *L*, and radius, *a*, with $ka << 1$ and $a << L$. As such, equation 1 may be rewritten with the standard thin wire kernel, $K(z - z')$,

$$E_z = \frac{1}{4\pi\omega\varepsilon}\left(k^2 + \frac{\partial^2}{\partial z^2}\right)\int_{-L}^{L} K(z-z')\,I(z')dz' \tag{4}$$

where

$$K(z-z') = \frac{e^{-jk\sqrt{(z-z')^2+a^2}}}{\sqrt{(z-z')^2+a^2}} \tag{5}$$

and

$$I(z) = 2\pi a\,J_z(z). \tag{6}$$

In order to solve for the total electric field, $E^t = E^i + E^s$, from a radiating object with incident electric field, E^i, and scattered electric field, E^s, equation 3 becomes

$$J_z = \frac{I(z)}{2\pi a} = \sigma\left(E_z^i + E_z^s\right). \tag{7}$$

By applying equation 4 as the scattered field, $E^s(z)$, in equation 7, and assuming a slice-gap voltage source for $E^i(z)$, a Hallén's integral equation is fully derived for the current distribution, *I(z)*, along a single thin wire of half-length, *L*, radius, *a*, and conductivity, σ, in Hanson (*3*) and results in

$$\int_{-L}^{L}\left(K(z-z') + \frac{\omega\varepsilon}{a\sigma}\frac{e^{-jk|z-z'|}}{k}\right)I(z')dz' = c_1\sin kz + c_2\cos kz - \frac{j2\pi\omega\varepsilon}{k}\sin k\,|\,z - z_0\,|. \tag{8}$$

Similarly, the current distribution for a bundle of thin wires composed of *N* wires of half-length, *L*, radius, *a*, and conductivity, σ, in Huang et al. (*9*) and results in

$$\int_{-L}^{L}\left(K_{Bundle}(z-z') + \frac{2\omega\varepsilon}{N\pi a\sigma}\frac{e^{-jk|z-z'|}}{k}\right)I(z')dz' = c_1\sin kz + c_2\cos kz - \frac{j2\pi\omega\varepsilon}{k}\sin k\,|\,z - z_0\,|. \tag{9}$$

For the bundle, the standard thin wire kernel, *K(z – z')*, is stated using a bundle radius, *R*, which also satisfies the thin wire criteria, *kR << 1* and *R << L*,

$$K_{Bundle}(z-z') = \frac{e^{-jk\sqrt{(z')^2+R^2}}}{\sqrt{(z')^2+R^2}}. \tag{10}$$

According to Huang et al. (*9*), only the current along the wires at the outermost region of the bundle will contribute to far-field radiation while radiation from the inner wires will effectively be shielded. Thus, the number of wires, *N*, in equation 9 should be limited to the outermost tubes in the bundle, N_{outer}.

With the current distribution along the thin wire dipole, I_z, solved for in terms of frequency, geometry, and material conductivity, a point matching MoM solution may be applied to equations 8 and 9 as detailed in Hanson (*3*). This simulation was carried out using MATLAB in order to compare the conductivity and current distribution of a copper wire, double-wall CNT, and multi-wall CNT bundle (thread) dipole antenna.

3.1.1.1 Conductivity

The dipole current distribution simulation described previously assumes a thin wire with a surface current density. Thus, the conductivity for the dipole material is determined for this particular case. This has been derived for a general CNT geometry in Maksimenko et al. (*17*) and for an infinitely thin SWNT and metal conductor in Hanson (*3*). For the case of a thin metal cylinder,

$$\sigma_{metal} = -j\frac{e^2 N_e}{m_e(\omega - j\upsilon)}, \tag{11}$$

where e is the elementary electron charge ($1.602*10^{-19}$ coulombs), m_e is the electron mass ($9.11*10^{-31}$ kg), N_e is the electron density, and υ is the relaxation frequency. The value of N_e changes depending on whether the metal cylinder is modeled with a geometry similar to a SWNT with an infinitely thin (N_e^{2d}) or finite (N_e^{3d}) wall thickness. In order to extend the comparison of this simulation to metal wire dipole antennas with realistic diameter sizes, the three-dimensional electron density, N_e^{3d}, will be used instead of the two-dimensional case, $N_e^{2d} = (N_e^{3d})^{2/3}$. For bulk copper, $N_e^{3d} \approx 8.46*10^{28}$ electrons/m^3 and $\upsilon \approx (2.47*10^{-14})^{-1}$.

For an infinitely thin SWNT with radius, a, the quantum conductivity is approximated as

$$\sigma_{SWNT} = -j\frac{2e^2 v_F}{\pi^2 \hbar a(\omega - j\upsilon)}, \tag{12}$$

where v_F is the Fermi velocity for a CNT (approximately $9.71*10^5$ m/s) and ħ is Plank's constant ($1.0546*10^{-34}$ m^{2}kg/s). The relaxation frequency of the SWNT is estimated as $\upsilon \approx (3*10^{-12})^{-1}$.

As noted earlier, the CNT thread used to fabricate dipole antenna prototypes for this investigation is composed of bundled MWNT structures. The conductivity must be adjusted to account for the multiple conductive paths offered by the multi-shell structures. According to Fikioris (*16*), MWNTs may be thought of as a set of N coaxial cylindrical SWNTs with intershell spacing of approximately 3.4 Å. Assuming that electrons are confined to flow axially along each shell with no cross-shell hopping, it has been estimated that the MWNT may be treated as a SWNT with an effective radius of $R^{eff} = (R_1 + R_2 + \ldots + R_N) / N$, with R_N being the radius of the outermost shell, and with an effective conductivity of

$$\sigma_{MWNT} = \sum_{q=1}^{N} \sigma_{SWNT}^{(q)} . \tag{13}$$

Specifically, the MWNT structures in the CNT thread are mainly double-wall (N = 2), and thus the conductivity of each CNT in the CNT bundle simulation will be approximated as

$$\sigma_{DWNT} \approx 2\sigma_{SWNT} . \tag{14}$$

It has been experimentally shown that a large tunneling resistance, on the order of MΩ, exists between neighboring nanotubes within a CNT bundle (*18*). Thus, each MWNT in the CNT thread simulation is assumed to be a parallel channel for electrons to flow with no cross-tube tunneling allowed. The CNT thread conductivity will scale with the number of MWNT conductive paths contained within the bundle. For this simulation, the CNT thread of radius, R, will be approximated as a square bundle of MWNTs of radius, a, with its cross-sectional length and width equal to the actual thread diameter, $2R$. For a densely-packed bundle with uniform nanotube distribution, the total number of CNTs may be approximated as (*19*)

$$N_W = \frac{2(R-a)}{x}; N_L = \frac{2(R-a)}{(\sqrt{3}/2)x} + 1 \tag{15}$$

$$N_{total} = N_W \cdot N_L - \frac{N_L}{2}; N_{outer} = 2 \cdot (N_W + N_L) \tag{16}$$

$$\sigma_{Bundle} \approx N_{total} \cdot \sigma_{DWNT}, \tag{17}$$

where x is the intertube spacing, from center to center. Assuming a van der Waals spacing of 3.4 Å between nanotubes, the intertube spacing becomes $x = 2a + 3.4$ Å. Since the approximation of the CNT thread as a square bundle will yield slightly larger values of N_{total} and N_{outer}, the simulated CNT thread dipole conductivity and radiated power will be slightly higher than the measured values of the actual prototypes. In order to bring the simulated results closer to that of a circular bundle, N_{total} and N_{outer} are scaled by the difference between the area of a circle inscribed within a square of side half-length, R,

$$\frac{A_{circle}}{A_{square}} = \frac{\pi R^2}{2R \cdot 2R} = \frac{\pi}{4}; N_{total} \approx \frac{\pi}{4} N_{total}; N_{outer} \approx \frac{\pi}{4} N_{outer}. \tag{18}$$

The simulated conductivity of 30-gauge copper wire, a double-wall CNT, and CNT thread and rope (multi-ply thread) is shown in figures 4 (real part, Re[σ]) and 5 (imaginary part, Imag[σ]). The copper wire radius is 127.5 µm, the single CNT radius is 5 nm, the 1-ply CNT thread radius is 12.5 µm, the 3-ply CNT rope radius is 37.5 µm, and the 3x3-ply (9-ply) CNT rope radius is 112.5 µm. It should be noted that while the conductivity for the copper wire and CNT thread cases is calculated in S/m, the accurate unit of conductivity for the individual double-wall CNT case is S since the SWNT is modeled as an infinitely thin tube.

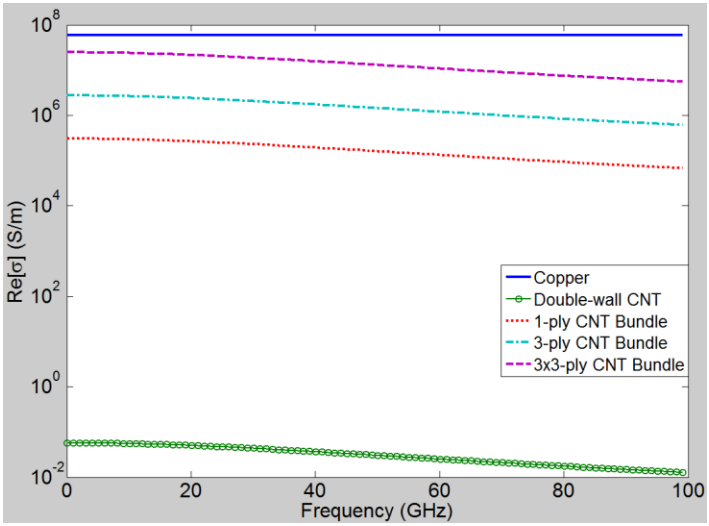

Figure 4. Real part of conductivity (log scale) vs. frequency for CNT thread and copper wire.

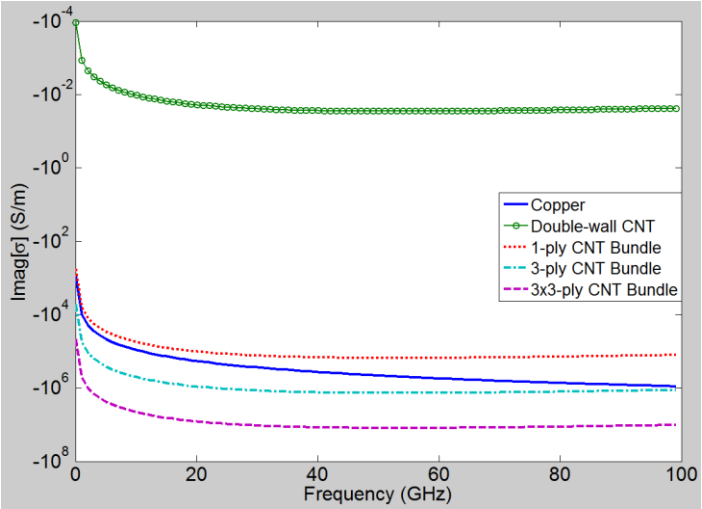

Figure 5. Imaginary part of conductivity (log scale) vs. frequency for CNT thread and copper wire.

The simulation data in figures 4 and 5 indicate that by increasing the diameter of the CNT thread (larger ply rope), and thus increasing the number of conducting channels within the structure, Re[σ] should improve to within one order of magnitude of bulk copper. The data also confirm previously reported simulation results that an individual CNT has a very low conductivity, on the order of 10e-2 S/m (*3*). Re[σ] of copper is accurately predicted to be ~5.9e7 S/m.

Fundamental differences between the conductivity of the CNT threads and 30-gauge copper wire become apparent when Imag[σ] is examined for each case. For copper, Imag[σ] remains two to three orders of magnitude lower than Re[σ] over the entire 0.1 to 100 GHz frequency range for copper, indicating that Re[σ] dominates and that the reactance losses in the structure attributed to Imag[σ] should be negligible. For each of the CNT threads/ropes, however, Imag[σ] is predicted to be zero to one order of magnitude less than Re[σ], with Imag[σ] approaching Re[σ] as the thread ply is increased. For the 3x3-ply CNT rope, Imag[σ] is predicted to be on the same order of magnitude as Re[σ]. These results indicate that significant reactance losses will arise as the diameter of the CNT rope is increased. The quantum effects (quantum capacitance and kinetic inductance) that occur due to the nanometer radius of the individual CNTs within the threads are the likely mechanisms behind this predicted increased reactance. For the 1-ply CNT thread, Re[σ] is predicted to be ~2 to 3e5 S/m, just two orders of magnitude less than copper, while Imag[σ] remains one order of magnitude lower than Re[σ] from 0.1 to 20 GHz. This indicates that the best electrical performance may be achieved by the 1-ply CNT thread until a strategy to mitigate the quantum reactance of the CNT elements is formulated.

3.1.1.2 Current Distribution

With the conductivity of the copper wire, double-wall CNT, and CNT threads accurately predicted, these values were applied to the MoM solution developed in section 3.1.1 to simulate and compare the current distribution across a λ/2 dipole antenna constructed from each of these

materials at a variety of frequencies. The current distribution for a 4-in-long dipole antenna, with resonant frequency, f_0, of 1.475 GHz is shown in figure 6.

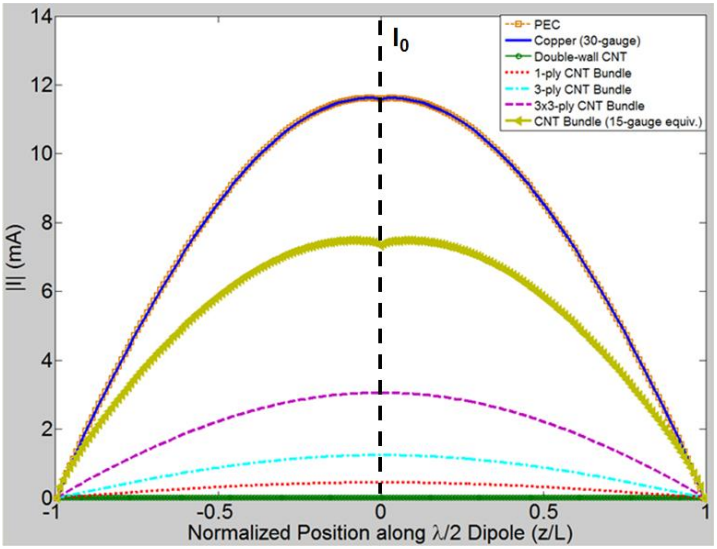

Figure 6. Comparison of current distribution (total magnitude) along λ/2 dipole antenna composed of different materials (f_0 = 1.475 GHz, L = 4 in).

The simulation accurately predicts the peak current maximum, I_0, for the 4-in perfect electric conductor (PEC) and copper dipole antenna to be ~11.8 mA based on Ohm's law using a 1-V applied signal and the known feedpoint impedance of a λ/2 dipole antenna, 73 + j42.5 Ω,

$$\left|\frac{V_0}{Z_{feedpoint}}\right| = |I_0| = \left|\frac{1V}{(73+j42.5)\,\Omega}\right| = 11.8\,mA. \tag{19}$$

The results indicate that each of the CNT thread dipole antennas will exhibit the traditional current distribution form of a λ/2 dipole antenna, with I_0 occurring at the center along the dipole structure (at z/L = 0), and that the value of I_0 should increase as the radius of the CNT thread increases despite the increased reactance losses predicted in the conductivity simulations. Since power delivered is proportional to I_0^2, it is possible to compare the approximate radiation efficiency of each CNT thread dipole with its copper dipole equivalent from

$$Radiation\ \ Efficiency\ \ Difference \propto 10 \cdot \log_{10}\left(\left(\frac{I_0^{CNT}}{I_0^{Copper}}\right)^2\right). \tag{20}$$

A hypothetical CNT rope with a radius equivalent to 15-gauge (r = 725 μm) copper wire was included in this simulation to compare the performance of an extremely large radius CNT rope with that of a typical copper wire. Note that at the present time, it is not possible to fabricate a CNT rope with radius equivalent to a 15-gauge wire. The results indicate that I_0 of such a CNT rope is ~65% that of a dipole fabricated with 30-gauge copper wire at 1.475 GHz. Applying this

ratio to equation 20 indicates that the radiation efficiency of the 15-gauge radius equivalent CNT rope dipole antenna may be ~3.8 dB less than that of the 30-gauge copper dipole antenna. I_0 for the 3x3-ply CNT rope dipole, which is approximately the same diameter as the 30-gauge copper wire (r = 127.5 μm), is ~26% that of a 30-gauge copper wire dipole. In turn, the radiation efficiency of the 3x3-ply CNT rope dipole is predicted to be ~11.6 dB less than that of the 30-gauge copper dipole. Evaluating the 3- and 1-ply CNT rope/thread dipoles in the same manner results in a predicted 19.4 dB lower radiation efficiency for the 3-ply rope and a massive 28-dB lower radiation efficiency for the 1-ply thread. Thus, despite a predicted increase in reactance losses as CNT thread diameter is increased, the radiation efficiency of a dipole antenna constructed from CNT thread is predicted to improve as rope diameter is increased. However, even if the CNT rope radius is increased to over five times the radius of the 30-gauge copper wire, the dipole antenna radiation efficiency is predicted to still be ~3.8 dB less for an operational frequency of 1.475 GHz.

Next, the CNT thread/rope dipole performance was examined in a higher frequency region by simulating the current distribution for a 3-mm-long λ/2 dipole antenna, with f_0 of ~50 GHz, as shown in figure 7. The CNT rope dipole with a radius equivalent to 15-gauge (r = 725 μm) copper wire was excluded from this simulation since the diameter ended up being on the order of the λ/2 dipole length at 50 GHz.

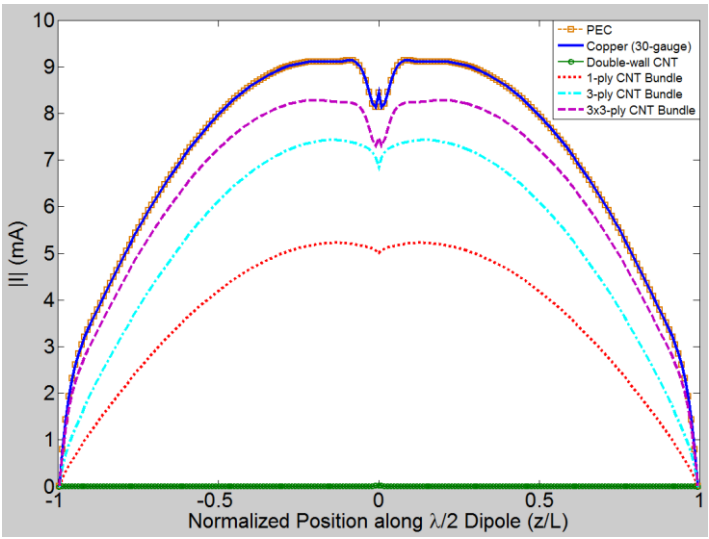

Figure 7. Comparison of current distribution (total magnitude) along λ/2 dipole antenna composed of different materials (f_0 = 50 GHz, L = 3 mm).

The results again confirm that each of the CNT thread/rope dipole antennas will exhibit the traditional current distribution form of a λ/2 dipole antenna, with I_0 occurring at the center along the dipole structure. Note that I_0 does not reach the ideal maximum of 11.8 mA for the PEC and copper cases since the dipole length, L, is exactly λ/2 and yields a true λ/2 dipole antenna, while in practice the optimum input impedance match to occurs when L is approximately 95% of λ/2

due to the fringing field end effects of the dipole structure. Also note that at this frequency, the delta function used as the slice-gap voltage source for the MoM simulation is noticeable as an artifact at the feedpoint (z/L = 0). The simulation again indicates that the value of I_0 should increase as the radius of the CNT thread increases.

Equation 20 was applied to these results to provide a radiation efficiency comparison for a λ/2 dipole at this frequency. The results show a marked performance improvement for the CNT thread at this frequency compared with its performance at 1.475 GHz, with the 1-, 3-, and 3x3-ply CNT thread/rope dipole antenna radiation efficiency predicted to be ~4.9, 1.8, and 0.9 dB lower than that of the 30-gauge copper wire dipole antenna, respectively. Thus, at higher frequencies, the RF performance tradeoff for using a CNT thread/rope dipole antenna in place of a copper wire antenna may be relatively low.

In figures 6 and 7, the individual double-wall CNT current distribution was many orders of magnitude lower than the other data sets and appeared to hug the bottom of the plot as a straight line. The magnified version of this data set is shown in figure 8, along with the simulated current distribution at f_0 = 50 GHz of a copper wire with comparable nanoscale radius, r = 5 nm.

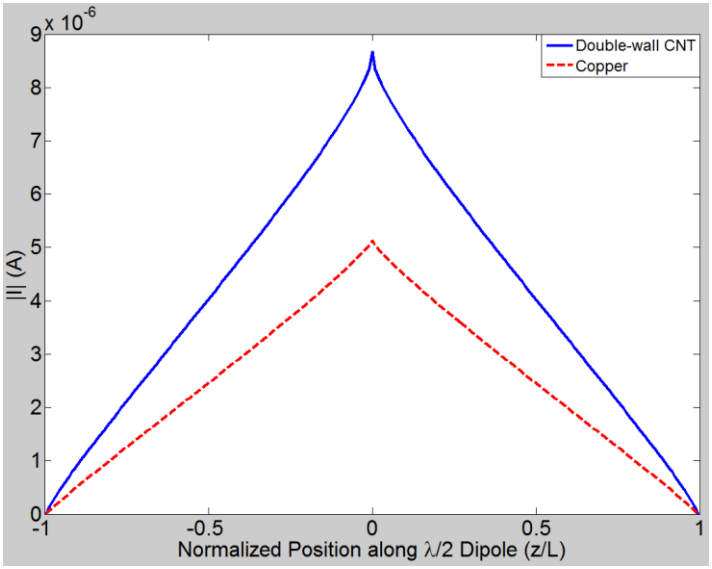

Figure 8. Comparison of current distribution (total magnitude) along λ/2 dipole antenna composed of nanoscale materials (f_0 = 50 GHz, L = 3 mm).

The magnitude of the current distribution for these nanoscale dipole antennas is predicted to be approximately three orders of magnitude lower than that of the CNT thread and 30-gauge copper wire dipole antennas. A triangular current distribution form is also displayed, similar to that of an electrically short (Hertzian) dipole antenna. By applying equation 20 to these results, the radiation efficiency is predicted to be ~60–70 dB lower than that of the 30-gauge copper wire for both the double-wall CNT and the nanoscale radius copper wire. However, these results reinforce the observation reported in Hanson (*3*) that an individual CNT will have a higher

radiation efficiency than a metallic nanowire of comparable radius and will thus serve as a better radiator.

In order to compare the radiation efficiency of the CNT thread/rope dipole antennas with the 30-gauge copper dipole antenna over a wide range of frequencies, the MoM simulation was run at discrete frequencies from 0.1 to 1 GHz and then from 1 to 100 GHz and the peak current, I_0, located at L = 0, was stored for each antenna type. The hypothetical CNT rope with a radius equivalent to 15-gauge (r = 725 μm) copper wire that was included in the previous 4-in dipole antenna simulation was included for all simulations from 0.1 to 1 GHz and was then excluded for the 1 to 100 GHz simulations in order to avoid the points at higher frequencies at which the dipole radius approaches its length.

As seen in figure 9, the radiation efficiency of larger ply CNT rope antennas (3x3-ply and rope with radius equivalent to 15-gauge wire) is predicted to increase more rapidly than the 1- and 3-ply thread/rope antennas from 100 MHz to 1 GHz. Below 500 MHz, radiation efficiency of the CNT thread/rope antennas is predicted to increase and diverge with that of the copper dipole antenna, regardless of rope radius. Above 500 MHz, the radiation efficiency of the large-ply CNT rope antennas increasingly become more competitive with that of the copper dipole antenna, albeit with a minimum power loss of 4–5 dB.

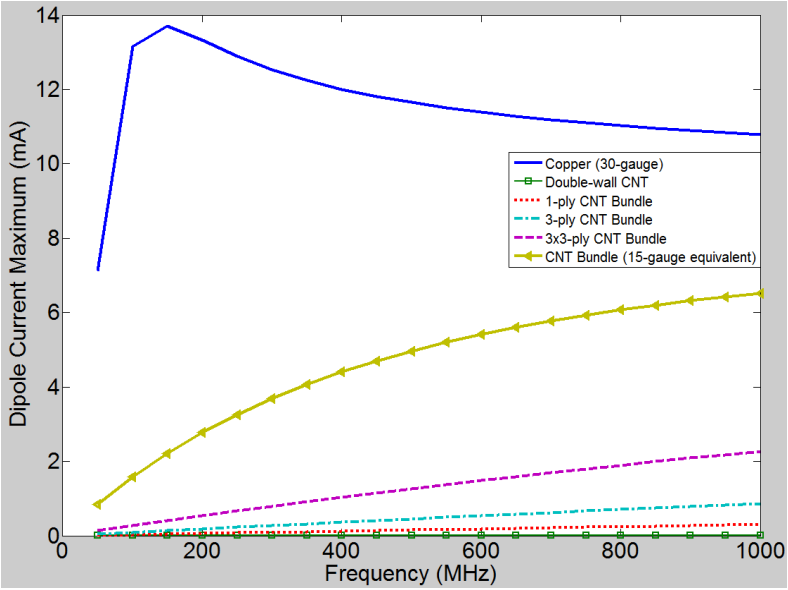

Figure 9. Current maximum (I_0) vs. frequency for λ/2 dipole antenna composed of different materials in MHz frequency range (L = λ/2).

The predicted dipole current maximum from 1 GHz to 100 GHz is shown in figure 10. For these higher frequencies, the radiation efficiency of the CNT thread/rope dipole antennas is predicted to become much more competitive with that of the 30-gauge copper wire above 10 GHz. Above 10 GHz, the radiation efficiency comparison relationship established by the previous 3-mm dipole antenna simulation remains relatively consistent up to 100 GHz. The radiation efficiency

of the 1-ply, 3-ply, and 3x3-ply CNT thread/rope antennas is predicted to be ~5.8, 2.5, and 1 dB lower than that of the 30-gauge copper wire, respectively.

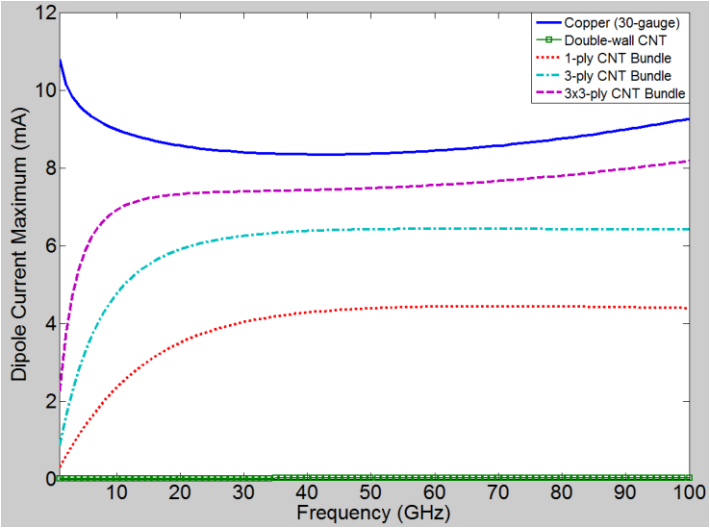

Figure 10. Current maximum (I_0) vs. frequency for λ/2 dipole antenna composed of different materials in GHz frequency range (L = λ/2).

It should be noted that while these conductivity and current distribution simulations include complex nanoscale impedance effects such as the quantum capacitance and kinetic inductance (through the quantum conductance model detailed in Burke et al. [*2*]), certain factors were approximated or unaccounted for and may limit the accuracy of the predicted results. One limitation to the applied CNT thread/rope simulation is that it does not account for defects in the individual CNTs, which may disrupt electron flow and act as a resistive barrier. Another approximation is that the model assumes that each CNT in the thread of radius, R, is the full length of the dipole, L = λ/2. However, an actual CNT thread dipole prototype is composed of individual MWNTs with radius, a = 10 nm, and average length of 500 μm bundled together by van der Waals forces and aligned axially. The gaps and junctions between individual CNTs may impact electrical conduction and cause electrons to hop laterally between nanotubes. Each of these approximations will likely increase the total resistance and reactance of the CNT thread, equal to both the longitudinal and lateral resistance of the nanotube bundle, and will consequently impact the thread conductivity and radiation efficiency. The amount that these approximations affect the accuracy of the simulations will be better quantified in the following section when the electrical and physical properties of CNT thread/rope samples are measured and compared with the simulation data.

3.1.2 Material Fabrication and Measurement

Working with the Nanoworld Laboratory at UC, a variety of CNT thread and rope samples were fabricated to apply to the construction of CNT thread/rope dipole antenna prototypes. The fabrication technique employed by UC to produce this thread is detailed in figure 11.

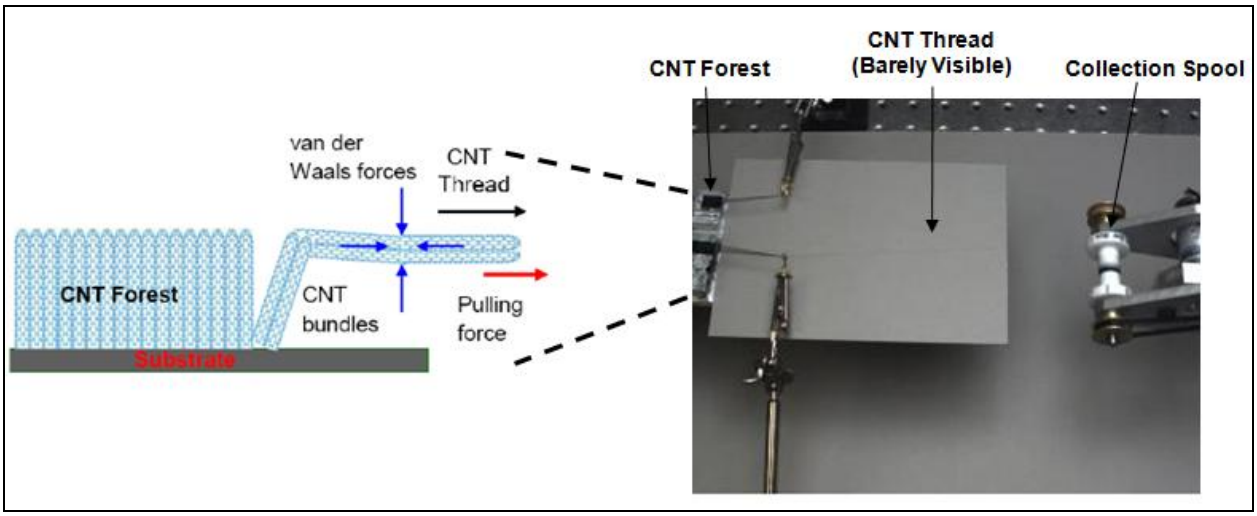

Figure 11. CNT thread fabrication technique at UC Nanoworld Laboratory (adapted from Mast [*15*]).

A dense array of vertically aligned MWNTs (typically 10–12 nm diameter double-wall CNTs) are grown using a CVD process on a 4-in silicon (Si) wafer with a density of ~0.03 gm/cm^3 and an average tube length of 500 µm. By means of a proprietary method, the MWNTs are collected and spun into a thread-like structure, with the individual nanotube bundles held together by van der Waals forces. The final 1-ply thread is typically 20–25 µm in diameter. By performing the same spinning process with multiple spools of 1-ply thread, a variety of larger-ply CNT rope was fabricated, including a 3-ply CNT rope and a 3x3-ply CNT rope (three 3-ply CNT ropes spun together). An additional post-processing technique of applying dimethyl sulfoxide (DMSO) to the CNT thread/rope samples was explored in order to enhance the thread conductivity and tensile strength. In this process, the capillary forces caused by the evaporation of the applied DMSO solvent draw the neighboring CNTs within the threads closer together and yield a denser thread structure. This process both reduces the CNT thread/rope diameter and enhances the ability to work with and handle the samples.

These standard and DMSO-densified samples were fabricated under ARL contract number W911QX11P0132 with contract period from April 2011–January 2012 and their physical and electrical properties were measured and analyzed. The samples were provided to ARL for the construction and measurement of CNT thread dipole antenna and meshed CNT thread patch antenna prototypes in year 2 of this DRI.

Images of the CNT thread/rope samples were captured using an environmental scanning electron microscope (ESEM), as shown in figures 12 through 14.

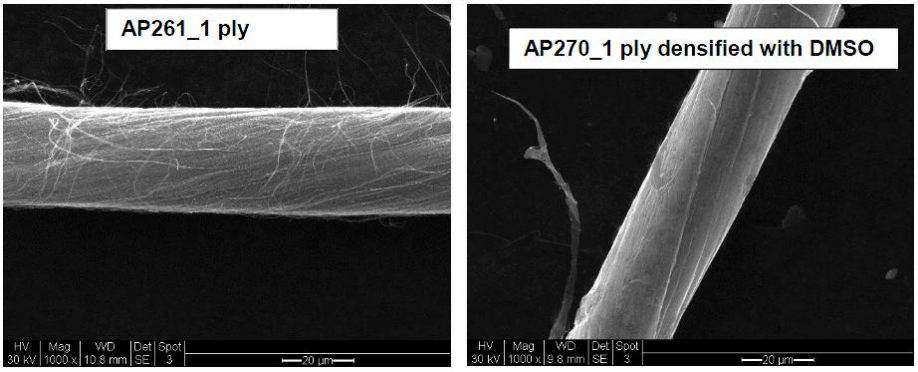

Figure 12. ESEM images of standard and DMSO densified 1-ply CNT thread.

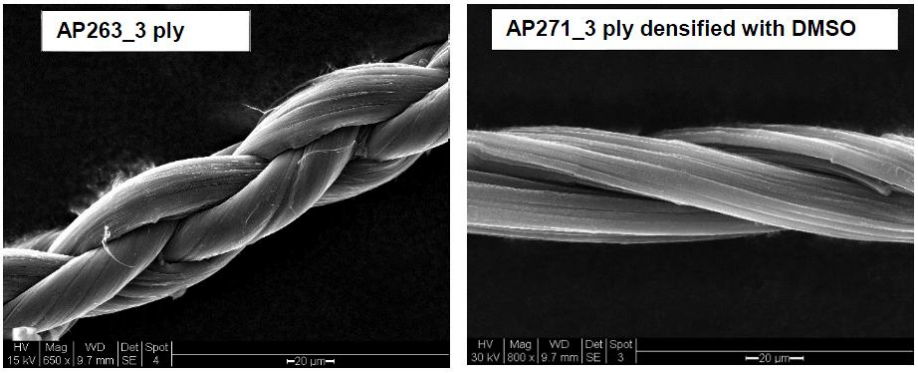

Figure 13. ESEM images of standard and DMSO densified 3-ply CNT rope.

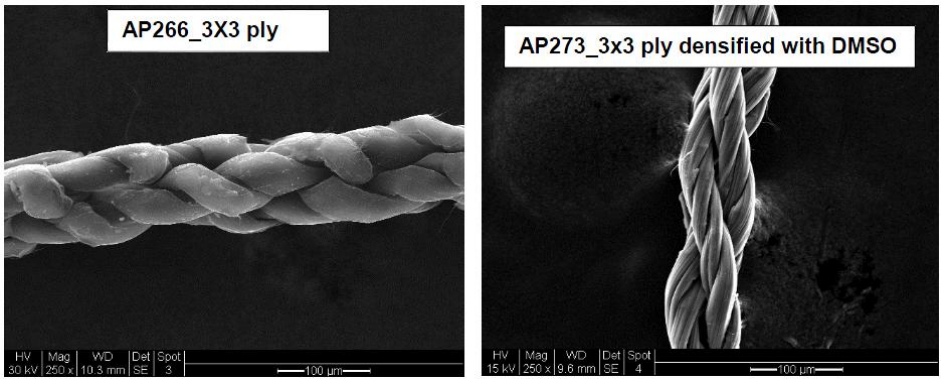

Figure 14. ESEM images of standard and DMSO densified 3x3-ply CNT rope.

In order to characterize the most important physical and electrical characteristics of the CNT thread/rope samples, the diameter, weight, conductivity, and tensile strength were acquired through measurement and analysis. The diameter, d, of each thread sample was evaluated by taking the average of four ESEM measurements. The DC resistance, R, of each of the CNT thread/rope samples was measured using a four probe technique. From these measurements and from the measured sample length, L, and cross-sectional area, A, the conductivity, σ, was calculated as

$$\rho = R \cdot \frac{A}{L} \quad ; \quad \sigma = \frac{1}{\rho} = \frac{L}{A \cdot R}. \tag{21}$$

While the exact weight of a short section of CNT thread could not be accurately measured, the researchers at UC quote a yield of approximately 5000 m of 1-ply CNT thread per 1 g of CNT array material used in the spinning process. This results in an estimated thread linear density of 0.0002 g/m for 1-ply CNT thread. This contrasts favorably with the approximate linear density of 30-gauge (0.453 g/m) and 15-gauge (14.73 g/m) copper wire. The measured average diameter and conductivity of each of the thread/rope samples and calculated weight (assuming a 4-in CNT dipole antenna, as simulated in section 3.1.1) is detailed in table 1. Estimated values for 15- and 30-gauge copper wire are also included for comparison.

Table 1. Material characterization of CNT thread/rope.

Prototype	d (μm)	L (mm)	R (Ω)	A (m^2)	ρ (Ω·m)	σ (S/m)	Weight of 4-in Dipole (mg)
1-ply CNT thread	29.2	3.699	409.0	6.68e-10	7.39e-05	1.35e04	0.0203
3-ply CNT rope	51.2	4.581	203.6	2.06e-09	9.14e-05	1.09e04	0.061
3x3-ply CNT rope	95.2	6.158	53.7	7.12e-09	6.21e-05	1.61e04	0.183
1-ply CNT thread w/ DMSO	27.1	7.245	424.6	5.77e-10	3.38e-05	2.96e04	0.0203
3-ply CNT rope w/ DMSO	37.8	5.984	200.1	1.12e-09	3.75e-05	2.67e04	0.061
3x3-ply CNT rope w/ DMSO	82.9	6.813	69.7	5.40e-09	5.53e-05	1.81e04	0.183
30-gauge Cu wire	255	NA	NA	NA	NA	5.9e07	46
15-gauge Cu wire	1450	NA	NA	NA	NA	5.9e07	1495

From these measurements, it can be seen that the diameter of the CNT thread/rope does not scale linearly with increased ply as it was applied in the simulations for section 3.1.1. The 3-ply CNT rope is just under two times the diameter of the 1-ply thread and the 3x3-ply (9-ply) rope is approximately three times the diameter of the 1-ply thread and just under two times the diameter of the 3-ply rope. This is due to the irregular braided intertwining of the 1-ply CNT threads that is visible in the ESEM images of the 3-ply and 3x3-ply CNT rope. The densification effect of the DMSO treatment on the CNT thread/rope samples is also apparent, with the diameter of each DMSO-treated sample reduced to ~80–90% of its original standard diameter.

The measured conductivity of the CNT thread/rope samples was found to be approximately two orders of magnitude lower than that predicted by the simulations from section 3.1.1 (10^4 vs. 10^6 S/m) and consistently three orders of magnitude lower than bulk copper. When the margin of error for the measured sample thread/rope diameter (and consequently the cross-sectional area) is considered, it can be concluded from these measurements that increasing the thread ply does not significantly enhance the sample conductivity and that each sample remains ~1–1.5e4 S/m.

However, the samples treated with DMSO exhibit an approximate 1.5 to 3 times increase in conductivity when compared with the untreated samples. This is likely due to the fact that the sample conductivity is heavily dependent upon the contact area existing between individual CNTs within the threads and that the DMSO densification technique increases this inter-tube contact area. This indicates that the DMSO densification procedure is a valuable post-processing technique that should be explored to further improve CNT thread conductivity. Among both the DMSO-treated and untreated samples, the thread resistance, R, is significantly reduced with increased thread ply, decreasing from ~415 Ω to 60 Ω as the ply is increased from 1- to 3x3-ply. This should be explored further to predict how to best minimize ohmic losses in antennas constructed from CNT thread/rope materials.

From this data and the simulation data of section 3.1.1, a weight versus radiation efficiency tradeoff comparison may be made between using CNT thread/rope versus copper wire for a dipole antenna. From figure 6, it was estimated from the simulated current maximum, I_0, of an 4-in $\lambda/2$ antenna ($f_0 \approx 1.475$ GHz) that the radiation efficiency of a 4-in length 1-, 3-, and 3x3-ply CNT thread/rope dipole antenna would be ~28, 19.4, and 11.6 dB lower, respectively, than that of a 30-gauge copper wire dipole antenna. At this frequency, the predicted losses using lower-ply CNT material would be much too large to be applied to an antenna design. However, for applications in which an 11–12 dB decrease (~93%) in radiation efficiency could be compensated for, the overall weight of the antenna may be reduced from 46 mg to 0.18 mg (~255 times) by employing 3x3-ply CNT thread versus 30-gauge copper wire. Despite this significant weight savings, the minimum predicted losses of ~11–12 dB at 1.475 GHz will likely be much too high for most applications to justify the use of CNT thread as a substitute for copper wire. However, at higher frequencies, the weight savings will be retained (albeit at a smaller overall order of magnitude) and the radiation efficiency losses are predicted to be much lower and more manageable. From figure 7, it was estimated that the radiation efficiency of a 3-mm-long 1-, 3-, and 3x3-ply CNT thread/rope dipole antenna radiation efficiency would be ~4.9, 1.8, and 0.9 dB lower, respectively, than that of the 30-gauge copper wire dipole antenna. Losses of this scale, particularly the <1 dB predicted loss for 3x3-ply CNT thread, could easily be compensated for in practical antenna applications. Thus, for a 0.9-dB drop in radiation efficiency (~18%), the antenna weight could be reduced ~250 times from 1.36 mg to ~0.54 μg. While this overall weight difference would be unnoticeable on a large-scale platform, it could still be applicable to severely weight restricted platforms such as micro-autonomous vehicles and make the weight contribution of the antenna negligible.

The tensile strength of the CNT thread/rope samples was also measured to compare the flexibility of the materials with copper (known tensile strength of ~170 to 220 MPa). Without DMSO treatment, the standard 1-ply CNT thread sample exhibited a tensile strength of ~78 MPa, as shown in figure 15. The standard 3- and 3x3-ply CNT rope samples demonstrated tensile strength of ~55 and 45 MPa, respectively. Contrary to what was expected to occur with increased sample ply, the tensile strength actually decreased as the ply was increased from 1-ply

to 3- and 3x3-ply. However, with DMSO treatment, the 1-ply CNT thread exhibited ~170 MPa tensile strength, approximately 2.5 times the tensile strength of the untreated 1-ply CNT thread, as shown in figure 16. The increased inter-tube contact area that was found to enhance the measured CNT thread conductivity is also the likely mechanism behind this significant increase in tensile strength.

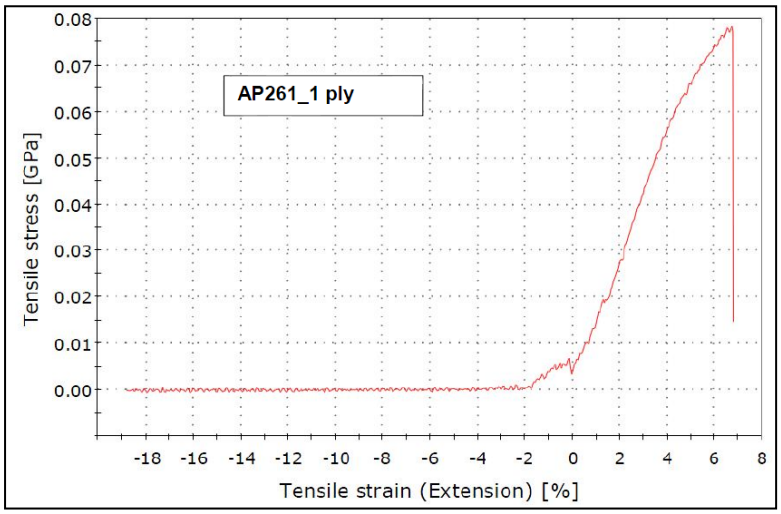

Figure 15. Measured tensile strength for standard 1-ply CNT thread sample.

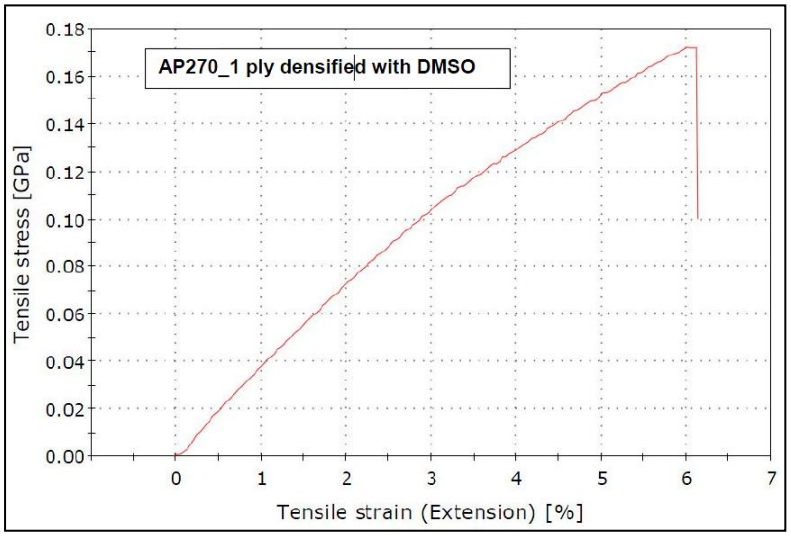

Figure 16. Measured tensile strength for DMSO densified 1-ply CNT thread sample.

Similar to the results for the untreated thread samples, the larger-ply DMSO treated CNT rope samples exhibited lower tensile strength as the ply was increased, being 136 MPa for the 3-ply rope (figure 17) and only 45 MPa for the 3x3-ply rope (figure 18). In figure 18, several curves are displayed and identified as Specimens 1 and 2. These curves belong to the initial sample strained by multiple tensile strength test runs. The reason for their appearance is that the tensile

instrument is designed to stop testing once the load goes 80% below the registered peak load. This indicates that an irreversible failure has occurred and the experiment is automatically discontinued. Interestingly, in the case of multi-ply CNT rope samples, the individual 1-ply threads within the rope do not undergo simultaneous rupture and some of them survive and avoid complete failure of the entire multi ply rope. This gives an opportunity to test the remaining intact rope structure again, which generates another stress-strain curve related to an "additional" Specimen 2. In general, the second run results in a lower measured tensile strength.

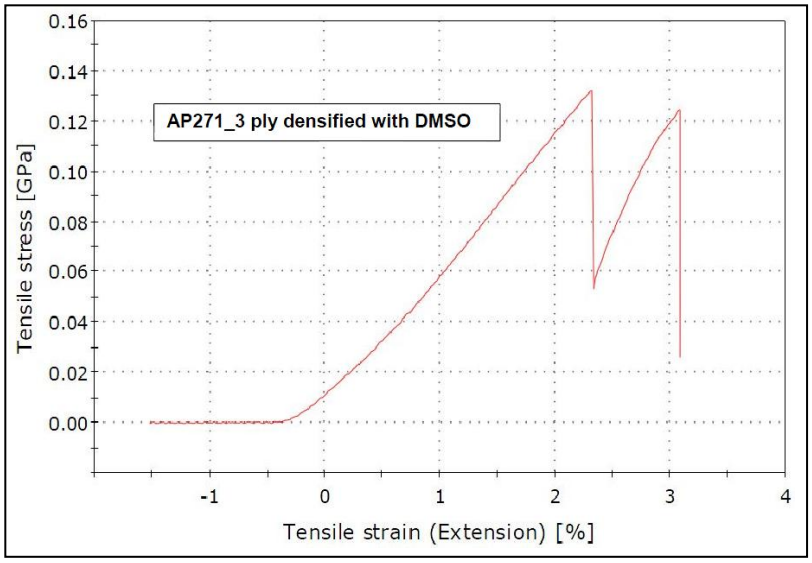

Figure 17. Measured tensile strength for DMSO densified 3-ply CNT rope sample.

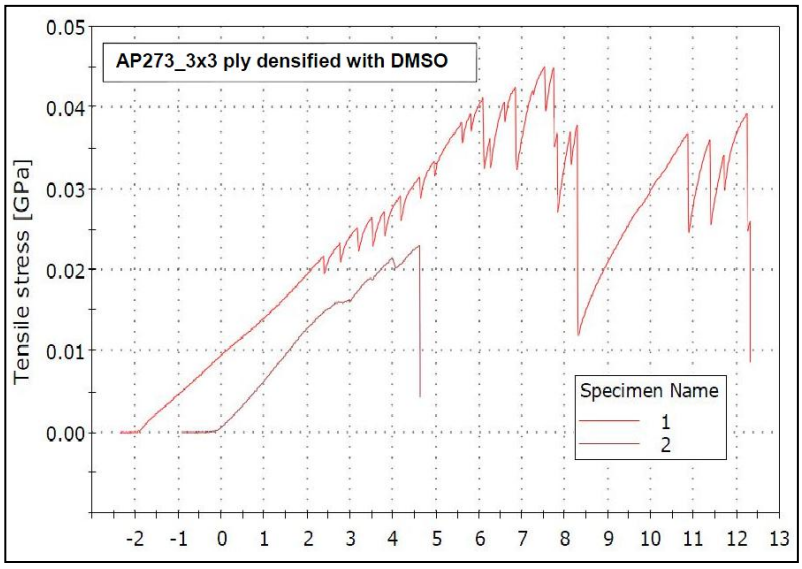

Figure 18. Measured tensile strength for DMSO densified 3x3-ply CNT rope sample.

These results indicate that the post-process DMSO treatment is an important step in strengthening the material. According to the researchers at UC, it is expected that by employing

thermal annealing as an additional post processing treatment to the CNT thread/rope, both the conductivity and tensile strength can be significantly improved. Early results from single-ply samples that are both DMSO-treated and thermally annealed have apparently demonstrated conductivity of ~1e6 S/m, very close to what was predicted in the simulations in section 3.1.1, and tensile strength of ~1 GPa. If these results can be consistently achieved and improved upon with future CNT thread samples, it should lead to a very attractive conductive material for RF applications.

3.2 ARL Multiwall Carbon Nanotube Array Growth Capabilities

Since 2007, ARL's Sensor and Electron Device Directorate (SEDD) has established the capability to grow SWNTs with an interest toward exploiting the semiconducting properties for electronic devices. However, for use in antenna applications, MWNTs and patterned MWNT bundles are desirable for antenna array applications. In order to best position ARL to research this area in the future, part of this DRI focused on the development of patterned MWNT growth capabilities using an existing low pressure CVD tool (currently used for graphene growth).

CNT growth requires the presence of nanometer-sized metal particles for use as a catalyst. Iron-family transition metals, namely, iron (Fe), nickel (Ni), and cobalt, make excellent catalyst materials primarily because they readily form solid solutions with carbon (*21, 22*). For MWNT growth, thin metal films, ranging from 10 to 100 Å thick, are used as the catalyst material with an aluminum thin film deposited as a support layer. When heated, the aluminum (Al) support layer readily oxidizes and forms clusters that prevent the metal from diffusing and forming large particles on the substrate (*23*).

For this work, Fe and Ni thin films were used as the catalyst material. First, a 50–75 Å Al film was deposited onto silicon dioxide (SiO_2)/Si wafers by e-beam evaporation. After deposition, the Al film was removed from the chamber and allowed to oxidize. The Al film was then placed in the e-beam deposition tool, and a thin layer of Fe or Ni was deposited. Film thickness for the Ni and Fe were 16 Å and 25 Å, respectively. The catalyst metals were deposited as a blanket film covering the entire wafer and/or patterned using standard photolithography lift-off techniques. The pattern contained squares, rectangles, and circles of sizes varying from 5 µm to 2 mm. The periodic nature of this pattern will be useful in a future effort to fabricate and test planar CNT bundle antenna arrays. An image of a patterned sample with Ni/Al bilayer deposition is shown in figure 19 (left image).

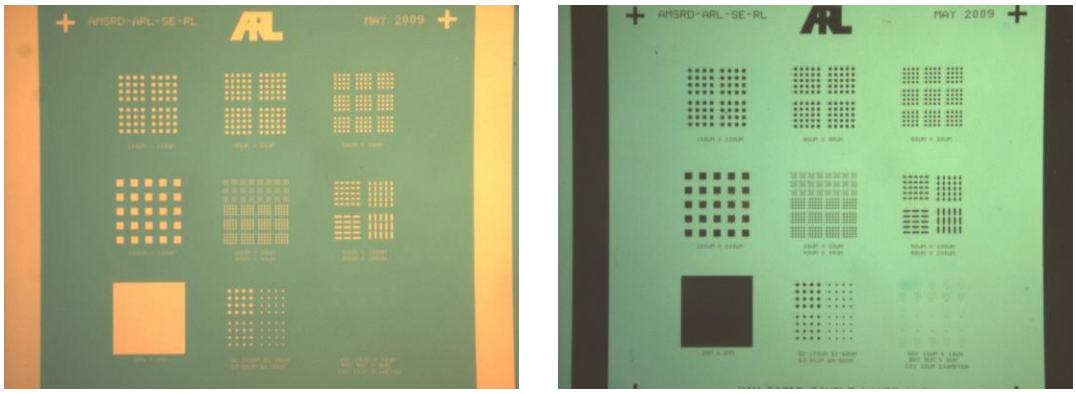

Figure 19. Two images of the patterned growth substrates before and after CNT growth. The first image shows the 16 Å Ni/75 Å Al thin film patterned on a SiO_2/Si substrate. The second image shows the patterned areas covered with black CNTs.

Once the catalyzed substrates were made, they were loaded into the low pressure chemical vapor deposition (LPCVD) tool furnace, and the system was pump downed to a base pressure less than 0.5 Torr. Hydrogen (H_2) and argon (Ar) were flowed into the furnace, and the target chamber pressure (100 to 400 Torr) was set. The furnace was heated to ~650–700 °C, and the catalyst films were annealed in the H_2/Ar atmosphere for 10–30 min. The growth phase began when the Ar was switched off, and ethylene, the carbon feedstock gas, was flowed into the furnace. After growth, the ethylene gas flow was terminated, and the system was cooled down to room temperature. The target pressure was maintained through the entire run. An image of the patterned sample after growth can be seen in figure 19 (right image). Dense groupings of CNTs appear black to the naked eye.

An Fe thin-film catalyst is typically preferred for MWNT growth (*24–26*); however, for these experiments, sustainable MWNT growth was not achieved using this material. No MWNT growth was observed for the patterned Fe thin films. MWNT growth was observed on the blanket Fe thin films; however, the tubes were not adhered well to the substrates and fell off the substrate upon movement. Prior to growth, the deposited catalyst film is oxidized due to ambient exposure. The pre-growth anneal in a H_2 environment is a necessary step to reduce the catalyst back to its elemental form and to allow formation of catalyst nanoparticles. Annealing time was shown to play a role in CNT formation. For all anneals performed for 15 min, no CNT growth was observed regardless of catalyst material. However, CNTs were deposited on the Ni catalyst when the time was doubled to 30 min. Increased anneal times were beneficial to promoting SWNT growth under atmospheric conditions using similar Ni/Al bilayer film thicknesses.

SEM images of CNT growth exclusively on the patterned Ni/Al areas can be seen in figure 20. A series of four images is shown from an array of 80 mm x 80 mm patterned squares, with each successive image taken at a higher magnification. The structure of the nanotube interaction/grouping is revealed as the magnification is increased. The nanotubes densely cover the patterned area and seem to be free from any excessive carbon build-up; however, they are not

vertical aligned as desired. CNTs of various diameters and lengths are observed although the total height of the entire nanotube carpet could not determined by the multiple images taken. Most likely, the nanotube carpet is no more than 1 μm in height as reported in the literature for nonaligned carbon nanotubes that exhibit similar morphologies (*27, 28*).

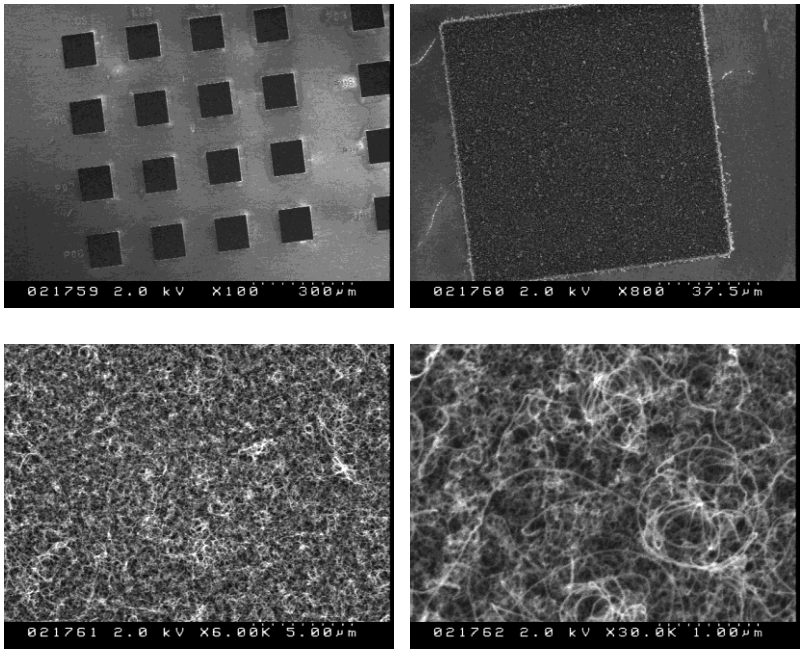

Figure 20. SEM images of MWNT growth on an array of 80 mm x 80 mm squares patterned with 16 Å Ni/75 Å Al bilayer. Images are taken in succession as the magnification increases and the CNT structure is revealed.

Raman spectroscopy was performed on the samples to provide insight into the general quality of the deposited nanotubes. A Renishaw inVia microscope with a 514 nm laser wavelength was used for this measurement. A typical Raman spectrum observed from the nanotubes can be seen in figure 21. For MWNTs, the important characteristic Raman features are the D and G peaks at ~1350 and ~1585 cm^{-1}, respectively. The G peak, which represents a stretching of the C-C band, is common to all graphitic materials, including graphene and some amorphous carbons. The D band indicates the presence of disorder found in sp^2-bonded carbon systems. For this figure, the D and G peak positions are 1342 and 1593 cm^{-1}, respectively, with an I_D/I_G ratio of 0.84. This value is typical for nonaligned CNTs; however, vertically aligned tubes generally have $I_D/I_G << 1$ although exceptions have been noted (*24, 28*). Sources for the large D peak can include defects in the tube as well as defects at the CNT tip-nanoparticle interface. The Raman spectra observed for these growths are similar to those reported by other researchers (*27, 28*), and the missing alignment of the CNTs is generally produced at lower growth temperatures.

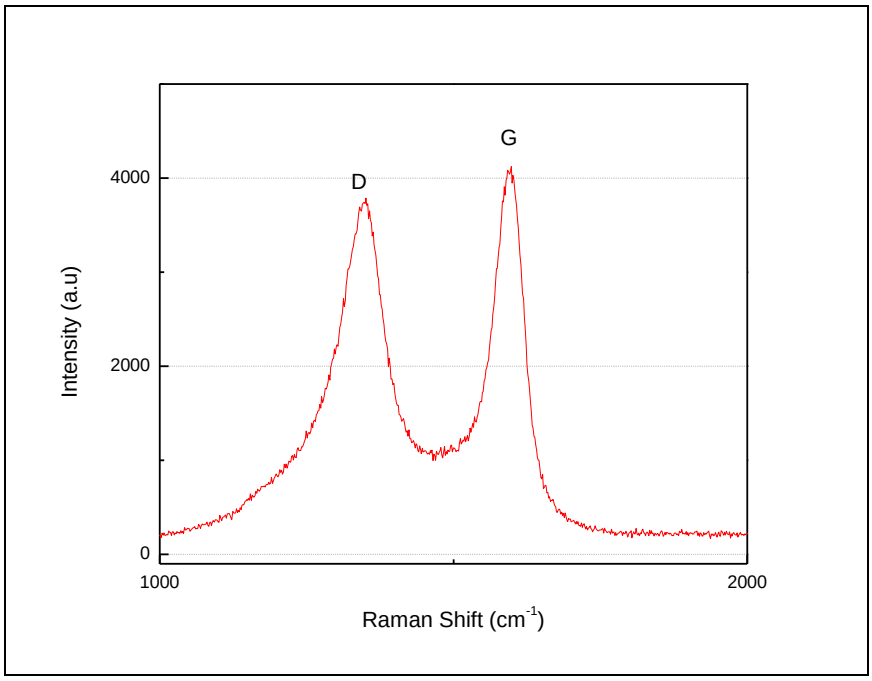

Figure 21. Typical Raman spectra taken from MWNTs grown from Ni/AL bilayer.

4. Conclusions and Future Work

In year 1 of this DRI, the application of CNT thread/rope to RF antenna designs was explored through conductivity and dipole antenna simulation and the measurement and analysis of physical and electrical characteristics of CNT thread/rope samples. The simulation results indicate that CNT thread/rope conductivity should improve with increased diameter (ply) and that the application of these materials as a half wavelength dipole antenna should yield manageable losses of less than 1 to 5 dB at RF frequencies above 10 GHz.

According to the measured results obtained from the CNT thread/rope samples fabricated by UC, it seems that the most significant physical benefit to be gained by employing CNT thread versus copper wire is a reduction in conductor weight. Contrary to what was expected from intuition and simulation results, the tensile strength and conductivity of the multi-ply CNT rope samples actually decreased with larger-ply rope and was less than that of the single-ply CNT thread samples. Thus, single-ply CNT thread should be focused on for future research. Applying a post-fabrication treatment of DMSO to the CNT threads was found to be an important step in enhancing the physical and electrical characteristics of the material. The tensile strength exhibited by the DMSO-treated single ply CNT thread was ~2.5 times greater than that exhibited by the untreated sample and was approximately the same as that of copper wire. With thermal annealing applied as an additional post-process treatment, it is expected that the conductivity should improve to at least 1e6 S/m (still lower than copper but more competitive) and the tensile

strength should improve to ~1 GPa (much higher than copper). Improvement of the tensile strength to far beyond that of copper will be an important step in justifying the use of CNT thread materials as a substitute for a traditional conductive material. As bulk CNT thread fabrication capabilities are refined and costs are lowered (typical cost in 2011 is ~$400 per gram of MWNT forest or 8 cents per meter of CNT thread), these materials should become an attractive alternative conductive material for weight-restricted and uniform-integrated Army antenna applications.

Additionally, the first steps were taken towards establishing patterned vertically aligned MWNT array fabrication capabilities at ARL. A variety of patterned CNT arrays were successfully fabricated on Si wafers, with pattern sizes ranging from 5 μm to 2 mm. Attempts at fabricating MWNT arrays using a Fe thin-film catalyst were ultimately unsuccessful since the nanotubes did not adhere well to the substrate. While future research will be needed to produce sustainable vertically aligned MWNT growth capabilities at ARL, the patterned CNT array fabrication capabilities developed under this program will be applicable to future Army research of planar CNT antenna arrays.

In year 2 of this DRI, a variety of fully fabricated CNT thread/rope dipole antennas will be measured and compared with a standard copper dipole antenna. The integration of this design into a textile substrate to produce a body-wearable antenna will also be explored. This will be the culmination of the CNT thread dipole prototype investigation from year 1 and will be a significant step towards demonstration of a Soldier uniform-integrated CNT thread antenna.

The work conducted in year 1 will also be built upon by exploring a more complex and novel CNT antenna structure comprised of interwoven CNT threads and ropes (multi-ply threads). The patch antenna has proven to be quite effective for a variety of Army applications, including terrestrial and satellite communications systems and various radar electronic scanning arrays due to its low-profile, planar structure, reasonable bandwidth of typically 10–20%, and excellent gain of typically 7 dBi. Previous research has shown that substituting a meshed conductive structure for the radiating patch and/or ground plane in place of a traditionally used solid conductive structure (e.g., copper patch) yields no significant change to the broadside antenna radiation pattern and small to moderate losses in gain and bandwidth depending on the density of the mesh (*20*). By applying interwoven CNT thread/rope to such a structure, it may be possible to construct a patch antenna capable of being easily integrated into a Soldier's uniform for applications in which weight and flexibility/durability are major concerns. For the initial prototype, only the patch structure will be fabricated using interwoven CNT threads/ropes constructed on a rigid, low-loss dielectric substrate with a copper ground plane/aperture layer. The focus of the investigation will be on how well the meshed CNT thread patch serves as the antenna radiator and what radiation performance tradeoffs (gain, bandwidth, radiation pattern) may arise from using such a design instead of a traditional solid metal patch. After this proof of concept, alternative designs will be explored in which both the patch and the ground plane/aperture layers are constructed from the interwoven CNT thread material and in which the

antenna is seamlessly integrated into a textile substrate (for body-worn applications). The meshed patch antenna will be explored through electromagnetic simulation using *Ansoft* High Frequency Structure Simulator (HFSS) and/or FEKO, and simulation results will be compared with measured results for model validation. With a validated model, it will be possible to determine the impact that the thread diameter and the number of threads in each interwoven column/row has on the radiation performance of the patch antenna. The goal will be to research the CNT meshed patch structure through simulation (full-wave and/or numerical), fabrication, and measurement. Simulation results will be compared with measured results for model validation. The over-arching goal of this research will be a flexible, lightweight, extremely durable CNT patch antenna for weight-restricted platforms and body-worn RF applications.

5. References

1. Kang, I. et al. Introduction to Carbon Nanotube and Nanofiber Smart Materials. *Composites Part B: Engineering* **2006**, *37* (6), 382–394.

2. Burke, P. J.; Li, S.; Yu, Z. Quantitative Theory of Nanowire and Nanotube Antenna Performance. *IEEE Transactions on Nanotechnology* **July 2006**, *5* (4), 314–334.

3. Hanson, G. W. Radiation Efficiency of Nano-radius Dipole Antennas in the Microwave and Far-infrared Regimes. *IEEE Antennas and Propag. Mag* **June 2008**, *50* (3), 66–77.

4. Zhou, Y.; Bayram, Y.; Du, F.; Dai, L.; Volakis, J. L. Polymer-carbon Nanotube Sheets for Conformal Load Bearing Antennas. *IEEE Trans. Antennas Propag.* **July 2010**, *58* (7), 2169–2175.

5. Yang, L.; Zhang, R.; Staiculescu, D.; Wong, C. P.; Tentzeris, M. M. A Novel Conformal RFID-enabled Module Utilizing Inkjet-printed Antennas and Carbon Nanotubes for Gas-detection Applications. *IEEE Antennas Wireless Propag. Let.* **2009**, *8*, 653–656.

6. Salahuddin, S.; Lundstrom, M.; Datta, S. Transport Effects on Signal Propagation in Quantum Wires. *IEEE Trans. Electron Devices* **Aug. 2005**, *52* (8), 1734–1742.

7. Raychowdhury, A.; Roy, K. Modeling of Metallic Carbon-nanotube Interconnects for Circuit Simulations and a Comparison with cu Interconnects for Scaled Technologies. *IEEE Trans. Comput.-Aided Des.* **Jan. 2006**, *25* (1), 58–65.

8. Plombon, J. J.; O'Brien, K. P.; Gstrein, F.; Dubin, V. M. High-frequency Electrical Properties of Individual and Bundled Carbon Nanotubes. *Appl. Phys. Let.* **2007**, *90*.

9. Huang, Y.; Yin, W.-Y.; Liu, Q. H. Performance Prediction of Carbon Nanotube Bundle Dipole Antennas. *IEEE Trans. Nanotech.* **May 2008**, *7* (3), 331–337.

10. Choi, S.; Sarabandi, K. Performance Assessment of Bundled Carbon Nanotube for Antenna Applications at Terahertz Frequencies and Higher. *IEEE Trans. Antennas Propag.* **March 2011**, *59* (3), 802–809.

11. Kimball, B.; Carlson, J. B.; Steeves, D.; Kemba, K.; Ren, Z.; Wu, P.; Kempa, T.; Benham, G.; Wang, Y.; Li, W.; Herczynski, A.; Rybczynski, J.; Rao, W.V.G.L.N. Diffraction Effects in Honeycomb Arrays of Multiwalled Carbon Nanotubes. *SPIE Proc.* **2004**, *5515*, 223–229.

12. Yao, Z.; Dekker, C.; Avouris, P. Electrical Transport Through Single-wall Carbon Nanotubes, in *Carbon Nanotubes; Topics in Applied Physics*, M. S. Desselhaus, G. Dresselhaus, and P. Avouris, Eds. Berlin, Germany: Springer-Verlag, vol. 80, pp. 147–171, 2001.

13. Iijima, S. Carbon Nanotubes: Past, Present, and Future. *Physica B.* **2002**, *323* (1–4), 1–5.

14. Nihei, M.; Kawabata, A.; Kondo, D.; Horibe, M.; Sato, S.; Awano, Y. Electrical Properties of Carbon Nanotube Bundles for Future via Interconnects. *Japanese Journal of Applied Physics* **2005**, *44* (4A), 1626–1628.

15. Mast, D. The Future of Carbon Nanotubes in Wireless Applications. *Antenna Systems/Short-Range Wireless Conference*, Sept. 2009.

16. Fikioris, G. On the Application of Numerical Methods to Hallén's Equation. *IEEE Trans. Antennas Propagat.* **March 2001**, *49* (3), 383–392.

17. Maksimenko, S. A.; Slepyan, G. Y.; Lakhtakia, A.; Yevtushenko, O., Gusakov, A. V. Electrodynamics of Carbon Nanotubes: Dynamic Conductivity, Impedance Boundary Conditions, and Surface Wave Propagation. *Phys. Rev. B* **Dec. 1999**, *60*, 17136–17149.

18. Stahl, H.; Appenzeller, J.; Martel, R.; Avouris, Ph.; Lengler, B. Intertube Coupling in Ropes of Single-wall Carbon Nanotubes. *Phys. Rev. Lett.* **Dec. 2000**, *85* (24), 5186–5189.

19. Srivastava, N.; Joshi, R. V.; Banerjee, F. Carbon Nanotube Interconnects: Implications for Performance, Power Dissipation and Thermal Management. *Electron Devices Meeting, 2005, IEDM Technical Digest*, 249–252, Dec. 2005.

20. Clasen, G.; Langley, R. Meshed Patch Antennas. *IEEE Trans. Antennas Propag.* **June 2004**, *52* (6), 1412–1416.

21. Homma, Y.; Kobayashi, Y.; Ogino, T.; Takagi, D.; Ito, R.; Jung, Y. J.; Ajayan, P. M. Role of Transition Metal Catalysts in Single-walled Carbon Nanotube Growth in Chemical Vapor Deposition. *J. Phys. Chem. B* **Oct. 2003**, *107* (44), 12161–12164.

22. Yuan, D. Y.; Ding, L.; Chu, H.; Feng, Y.; McNicholas, T. P.; Liu, J. Horizontally Aligned Single-walled Carbon Nanotube on Quartz From a Large Variety of Metal Catalysts. *Nano Letters* **July 2008**, *8* (8), 2576–2579.

23. Shin, K. Y.; Su, H. C.; Tsai, C. H. In Situ Growth of Single-walled Carbon Nanotubes by Bimetallic Technique With/Without Dielectric Support for Nanodevice Application. *IEEE Journal of Vacuum Science and Technology B* **Jan. 2006**, *24* (1), 358–361.

24. Hasegawa, K.; Noda, S. Millimeter-tall Single-walled Carbon Nanotubes Rapidly Grown With and Without Water. *ACS Nano* **2011**, *5* (2), 975–984.

25. Manohara, H. M.; Bronikowski, M. J.; Hoenk, M.; Hunt, B. D.; Siegel, P. H. High-current-density Field Emitters Based on Arrays of Carbon Nanotube Bundles. *Journal of Vacuum Science and Technology B* **2005**, *23* (1), 157–161.

26. Bronikowski, M. J.; Manohara, H. M.; Hunt, B. D. Growth of Carbon Nanotube Bundle Arrays on Silicon Surfaces. *Journal of Vacuum Science and Technology A* **2006**, *24* (4), 1318–1322.

27. Pal, S. K.; Talapatra, S.; Kar, S.; Ci, L.; Vajtai, R.; Borca-Tasciuc, T.; Schadler, L. S.; Ajayan, P. M. Time and Temperature Dependence of Multiwalled Carbon Nanotube Growth on Inconel 600. *Nanotechnology* **2008**, *19*.

28. Crossley, B. L. Carbon Nanotube Field Emission Arrays. Ph.D. dissertation, Air Force Institute of Technology, 2011.

6. Transitions

The goal of this research is to ultimately transition flexible, lightweight, durable antenna designs constructed from carbon nanotube materials to weight-restricted Army platforms (e.g., unmanned aerial vehicles [UAVs], micro-autonomous vehicles) and body-worn/textile integrated RF applications.

The research performed for year 1 of this DRI has produced a conference paper/presentation, a Technical Assessment Board (TAB) review poster, and a patent application (pending/accepted for process), and will likely result in at least one peer-reviewed journal publication (pending), as follows:

- Keller, S. D.; Zaghloul, A. I.; Shanov, V.; Schulz, M. J.; Mast, D. B. Simulation of carbon nanotube thread dipole antennas, *2011 USNC/URSI National Radio Science Meeting Proceedings*, July 2011. (paper and presentation)
- 2011 ARL TAB Review Poster, Lightweight, Durable Army Antennas Using Carbon Nanotube Technology.
- Patent pending on *Nanofabric* antenna array, ARL 10-38 - Nano-Fabric Antenna.
- Keller, S. D.; Zaghloul, A. I.; Shanov, V.; Schulz, M. J.; Mast, D. B. Simulation and measurement of carbon nanotube thread dipole antennas, IEEE Antennas and Wireless Propagation Letters [pending].

List of Symbols, Abbreviations, and Acronyms

Al	aluminum
Ar	argon
ARL	U.S. Army Research Laboratory
CNT	carbon nanotube
CVD	chemical vapor deposition
DMSO	dimethyl sulfoxide
DRI	Director's Research Initiative
ESEM	environmental scanning electron microscope
Fe	iron
H_2	hydrogen
HFSS	High Frequency Structure Simulator
LPCVD	low pressure chemical vapor deposition
MoM	method of moments
MWNT	multiwall CNT
Ni	nickel
PEC	perfect electric conductor
RF	radio frequency
SEDD	Sensor and Electron Devices Directorate
Si	silicon
SiO_2	silicon dioxide
SWNT	single-wall CNT
TAB	Technical Assessment Board
UAV	unmanned aerial vehicle
UC	University of Cincinnati

No of. Copies	Organization
1 PDF	DEFENSE TECH INFO CTR ATTN DTIC OCA 8725 JOHN J KINGMAN RD STE 0944 FT BELVOIR VA 22060-6218
18 HCS 1 CD	US ARMY RSRCH LAB ATTN IMNE ALC HRR MAIL & RECORDS MGMT ATTN RDRL CIO LL TECHL LIB ATTN RDRL CIO MT TECHL PUB ATTN RDRL D ATTN RDRL SER L B NICHOLS ATTN RDRL SER L B PIEKARSKI ATTN RDRL SER L M DUBEY ATTN RDRL SER M A ZAGHLOUL ATTN RDRL SER M E ADLER ATTN RDRL SER M S KELLER (7 HCS, 1 CD) ATTN RDRL SER M S WEISS ATTN RDRL SER P AMIRTHARAJ ADELPHI MD 20783-1197

TOTAL: 20 (1 PDF, 18 HCS, 1 CD)

INTENTIONALLY LEFT BLANK.